INTERNATIONAL JOURNAL FOR NUMERICAL METHODS IN FLUIDS
Int. J. Numer. Meth. Fluids **28**: 523–540 (1998)

NON-REFLECTING BOUNDARY CONDITIONS APPLICABLE TO GENERAL PURPOSE CFD SIMULATORS

HANS-CHRISTEN SALVESEN*,[1] AND RUNE TEIGLAND[2]

Christian Michelsen Research A/S, Fantoftveien 38, PO Box 3, N-5036 Fantoft, Norway

SUMMARY

In simulations of propagating blast waves the effects of artificial reflections at open boundaries can seriously degrade the accuracy of the computations. In this paper, a boundary condition based on a local approximation by a plane traveling wave is presented. The method yields small artificial reflections at open boundaries. The derivation and the theory behind these so-called plane-wave boundary conditions are presented. The method is conceptually simple and is easy to implement in two and three dimensions. These non-reflecting boundary conditions are employed in the three-dimensional computational fluid dynamics (CFD) solver FLACS, capable of simulating gas explosions and blast-wave propagation in complex geometries. Several examples involving propagating waves in one and two dimensions, shock tube and an example of a simulation of a propagating blast wave generated by an explosion in a compressor module are shown. The numerical simulations show that artificial reflections due to the boundary conditions employed are negligible. © 1998 John Wiley & Sons, Ltd.

KEY WORDS: non-reflecting boundary conditions; numerical simulation; compression wave

1. INTRODUCTION

When considering the consequences of gas explosions on offshore facilities, the emphasis is on the consequences in the area where the gas release would occur and is ignited. The possible consequences in the direct surroundings of such areas should also be considered. Blast waves generated by the initial explosion would propagate towards the living quarters or accommodation module, bridges connecting two neighbouring platforms, fire protection screens, life boats, etc. and possibly cause substantial damage there. Simulation tools to take into account these effects are needed. The computational fluid dynamics (CFD) simulator FLACS [1,2] is capable of simulating gas explosions and blast-wave propagation in obstructed, complex geometries.

The FLACS simulator can be run with several numerical blocks. The explosion takes place in the central block. The so-called FLACS solver is used here, and the averaged Navier–Stokes equations are solved, including the effects of turbulence and combustion. A finite volume discretization scheme is employed together with the SIMPLE [3] solution strategy where the momentum and continuity equations are solved in a segregated manner. A standard upwind scheme is used in the computation of the convective terms. The SIMPLE solution method belongs to the class of pressure correction methods, which are popular in the primitive variable

* Correspondence to: Christian Michelsen Research A/S, Fantoftveien 38, PO Box 3, N-5036 Fantoft, Norway.
[1] E-mail: Hans-Christen.Salvesen@cmr.no
[2] E-mail: Rune.Teigland@cmr.no; present address: AMES Department, UC San Diego, La Jolla, USA.

CCC 0271–2091/98/130523–18$17.50

Received July 1996
Revised December 1996

computation of complex industrial flows. The methods use a predictor-corrector approach to the solution of the Navier–Stokes equations and is a widely used method in CFD codes. It is a robust methodology applicable for complex, turbulent, reactive flows and it is potentially applicable to all regimes, from incompressible to supersonic flows.

Blast waves will propagate outward from the center of the explosion and into surrounding numerical blocks. If simulation of combustion is not important in such a block, the so-called blast solver can be used. Then the Euler equations in primitive variable form are solved based on the pressure correction method ICE [4,5], and using an explicit FCT method [6] in the calculation of the convection terms. This blast solver saves both execution time and memory in comparison with the fully implicit approach adopted in the FLACS solver.

After some time, depending on the size of the computational domain and the scenario, the blast waves reach the boundary of the computational domain. The computational domain is finite, and boundary conditions must be imposed at the edges of the grid. In general, a part of the boundary is an open boundary. These boundary conditions can generate spurious fluctuations that render the computational solution entirely unacceptable. Different boundary conditions for unsteady compressible flows have been proposed [7]. One such class of methods is based on quasi-one-dimensional characteristics, e.g. Reference [8].

In the present work, boundary conditions giving negligible artificial reflections at the open boundary of the computational domain are presented. These so-called plane-wave boundary conditions have been implemented in the three-dimensional FLACS simulator. The theory and derivation of these conditions are explained, and a comparison with the boundary conditions presented in Reference [9] is shown. The numerical results are presented here, simulating several problems involving propagating waves as well as a blast wave arising from an explosion in a compressor module.

It should be noted that more efficient methods exist for the solution of the Euler equations, e.g. Riemann type solvers. However, our emphasis is on presenting the plane-wave boundary conditions and implementing them in the CFD code FLACS, used for simulation of gas explosions and blast-wave propagation in complex geometries.

2. LOCAL APPROXIMATION BY A PLANE TRAVELING WAVE AT AN OPEN BOUNDARY

The one-dimensional Euler equations for an inviscid, perfect gas, are given in conservative form by

$$\frac{\partial \rho}{\partial t} + \frac{\partial}{\partial x}(\rho u) = 0, \tag{1}$$

$$\frac{\partial}{\partial t}(\rho u) + \frac{\partial}{\partial x}(\rho u^2 + p) = 0, \tag{2}$$

$$\frac{\partial}{\partial t}(\rho e) + \frac{\partial}{\partial x}(\rho e u + u p) = 0, \tag{3}$$

representing conservation of mass, momentum, and energy, respectively. Here, e is the total energy per unit mass,

$$e = \varepsilon + \frac{1}{2}u^2, \tag{4}$$

ε is the internal energy per unit mass, related to the pressure p by

$$p = (\gamma - 1)\,\rho\varepsilon. \tag{5}$$

In primitive variable form the Euler equations can be rewritten as the non-linear system

$$\frac{\partial V}{\partial t} + A\,\frac{\partial V}{\partial x} = 0, \tag{6}$$

where

$$V = \begin{pmatrix} \rho \\ u \\ p \end{pmatrix}, \tag{7}$$

$$A = \begin{pmatrix} u & \rho & 0 \\ 0 & u & 1/\rho \\ 0 & \rho c^2 & u \end{pmatrix}, \tag{8}$$

and $c = \sqrt{\gamma p/\rho}$ is the speed of sound. The characteristic values (eigenvalues) of the matrix A are

$$\lambda_1 = u - c, \tag{9}$$

$$\lambda_2 = u, \tag{10}$$

$$\lambda_3 = u + c. \tag{11}$$

The non-linear system Equation (6) can be transformed to the set of characteristic equations

$$\frac{\partial p}{\partial t} - \rho c\,\frac{\partial u}{\partial t} + \lambda_1\left(\frac{\partial p}{\partial x} - \rho c\,\frac{\partial u}{\partial x}\right) = 0, \tag{12}$$

$$\frac{\partial p}{\partial t} - c^2\,\frac{\partial \rho}{\partial t} + \lambda_2\left(\frac{\partial p}{\partial x} - c^2\,\frac{\partial \rho}{\partial x}\right) = 0, \tag{13}$$

$$\frac{\partial p}{\partial t} + \rho c\,\frac{\partial u}{\partial t} + \lambda_3\left(\frac{\partial p}{\partial x} + \rho c\,\frac{\partial u}{\partial x}\right) = 0. \tag{14}$$

Following Thompson [9], incoming modes are set to zero at an open boundary. Consider subsonic flow with an open boundary in the positive x-direction. Then the eigenvalue $\lambda_1 = u - c$ is directed inward, and the non-reflecting condition demands

$$\frac{\partial p}{\partial x} - \rho c\,\frac{\partial u}{\partial x} = 0. \tag{15}$$

Thus the characteristic Equation (12) is reduced to

$$\frac{\partial p}{\partial t} - \rho c\,\frac{\partial u}{\partial t} = 0. \tag{16}$$

Furthermore, if the eigenvalue $\lambda_2 = u$ is directed inward, $u < 0$, the non-reflecting condition demands

$$\frac{\partial p}{\partial x} - c^2\,\frac{\partial \rho}{\partial x} = 0, \tag{17}$$

and the characteristic Equation (13) is reduced to

$$\frac{\partial p}{\partial t} - c^2 \frac{\partial \rho}{\partial t} = 0. \tag{18}$$

When Equations (13)–(16) are linearized according to the approximation of linear acoustics, the resulting equations can easily be solved. The general solution is that of a plane wave traveling in the positive x-direction, as shown below.

The dependent variables are written as

$$p = p_0 + p', \tag{19}$$

$$\rho = \rho_0 + \rho', \tag{20}$$

$$u = u_0 + u', \tag{21}$$

$$c = c_0 + c', \tag{22}$$

where the primed variables represent the acoustic disturbance from the ambient state. It is assumed that the fluid is a homogeneous, quiescent medium of wave propagation, i.e. all ambient quantities are independent of position and time, and the ambient velocity is zero, $u_0 = 0$. The expressions in Equations (19)–(22) are inserted into (13)–(16), and in the linear approximation terms of second- or higher-order are discarded. Terms with one primed variable are of first-order, terms with two primed variables are of second-order, etc.

The linearized equations are given by

$$\frac{\partial}{\partial x}(p' - \rho_0 c_0 u') = 0, \tag{23}$$

$$\frac{\partial}{\partial t}(p' - \rho_0 c_0 u') = 0, \tag{24}$$

$$\frac{\partial}{\partial t}(p' - c_0^2 \rho') = 0, \tag{25}$$

$$\frac{\partial}{\partial t}(p' + \rho_0 c_0 u') + c_0 \frac{\partial}{\partial x}(p' + \rho_0 c_0 u') = 0. \tag{26}$$

Integrating Equations (23) and (24) shows that $(p' - \rho_0 c_0 u')$ equals an arbitrary constant. Assuming that the ambient state is defined, so that $u' \equiv 0$ corresponds to $p' \equiv 0$, this constant is set to zero. Thus

$$u' = \frac{p'}{\rho_0 c_0}, \tag{27}$$

and Equation (26) can be rewritten as

$$\frac{\partial p'}{\partial t} + c_0 \frac{\partial p'}{\partial x} = 0, \tag{28}$$

being a linear advection equation for p'. The general solution of this equation is

$$p' = f\left(t - \frac{x}{c_0}\right), \tag{29}$$

where the function f is arbitrary.

Integrating Equation (25) one sees that

$$p' - c_0^2 \rho' = h(x), \tag{30}$$

where h is an arbitrary function. Seeking wave-like solutions for ρ', $h(x) \equiv 0$ is set, so that

$$\rho' = \frac{p'}{c_0^2}, \tag{31}$$

and the linearized version of Equation (17) is satisfied (no incoming mode for the eigenvalue λ_2). The relation in Equation (31) can also be deduced by assuming constant entropy in the thermodynamic relation

$$p = p(\rho, s_0), \tag{32}$$

so that the pressure is a function of the density only. A Taylor expansion in ρ' gives

$$p_0 + p' = p(\rho_0 + \rho', s_0) = p_0 + \left(\frac{\partial p}{\partial \rho}\right)_{s_0} \rho' + O((\rho')^2). \tag{33}$$

Neglecting terms of second- or higher-order in the primed variables, and recognizing that $c_0^2 = (\partial p/\partial \rho)_{s_0}$ [10], the Taylor expansion in Equation (33) leads to the relation in Equation (31).

To summarize, the general solution of the linearized characteristic equations, assuming that there are no incoming modes, is that of a plane traveling wave as seen from Equations (27), (29) and (31).

Thompson [9] applied the system of quasi-linear characteristic Equations (12)–(14) directly to obtain non-reflecting boundary conditions. Conditions based on the general solution of the linearized equations were developed in this study. These conditions are easy to generalize to three space dimensions, and numerical testing (see Section 4) shows that for outgoing blast waves these conditions give negligible reflections at an open boundary.

In three space dimensions, a single plane traveling wave is described by the primary variables

$$p = p_0 + f\left(t - \frac{\mathbf{l}\cdot\mathbf{x}}{c_0}\right), \tag{34}$$

$$\rho = \rho_0 + \frac{p - p_0}{c_0^2} = \rho_0 + \frac{f(t - (\mathbf{l}\cdot\mathbf{x})/c_0)}{c_0^2}, \tag{35}$$

$$\mathbf{u} = \frac{\mathbf{l}}{\rho_0 c_0}(p - p_0) = \frac{\mathbf{l}}{\rho_0 c_0} f\left(t - \frac{\mathbf{l}\cdot\mathbf{x}}{c_0}\right), \tag{36}$$

where, as before, p_0 is the ambient pressure, ρ_0 is the ambient density, c_0 is the speed of sound corresponding to the ambient state, the function f is arbitrary, and $\mathbf{l}$ is the unit vector in the direction which the plane wave propagates. A derivation of these results is found in e.g. Reference [10].

If the primary variables are known at $\mathbf{x} = \mathbf{0}$, $t = 0$, values of nearby positions in both space and time may be approximated by a Taylor expansion, provided that the function f is smooth enough

$$p(\mathbf{x}, t) = p(0, 0) + f'(0)\left(t - \frac{\mathbf{l}\cdot\mathbf{x}}{c_0}\right) + O\left(t^2, \frac{|\mathbf{x}|^2}{c_0^2}\right), \tag{37}$$

$$\rho(\mathbf{x}, t) = \rho(0, 0) + \frac{f'(0)}{c_0^2}\left(t - \frac{\mathbf{l}\cdot\mathbf{x}}{c_0}\right) + O\left(t^2, \frac{|\mathbf{x}|^2}{c_0^2}\right), \tag{38}$$

$$\mathbf{u}(\mathbf{x}, t) = \mathbf{u}(\mathbf{0}, 0) + \mathbf{l}\left(\frac{f'(0)}{\rho_0 c_0}\left(t - \frac{\mathbf{l}\cdot\mathbf{x}}{c_0}\right) + O\left(t^2, \frac{|\mathbf{x}|^2}{c_0^2}\right)\right). \tag{39}$$

If the derivative $f'(0)$ and the wave propagation vector $\mathbf{l}$ are not known in advance, they can be determined from

$$\frac{\partial}{\partial t}\mathbf{u}(\mathbf{0}, 0) = \mathbf{l}\frac{f'(0)}{\rho_0 c_0}, \tag{40}$$

$$|\mathbf{l}| = 1, \tag{41}$$

and the sign of $\partial/\partial t\,\rho(\mathbf{0}, 0)$ being the sign of $f'(0)$. Equation (40) is obtained here by differentiation of Equation (36). The philosophy when applying this to open boundary conditions in numerical calculations is as follows. Assume that the flow field close to the open boundary may be locally approximated by a plane wave. Apply the Taylor expansions in Equations (37)–(39) to obtain approximations of the primary variables for the next time step at the boundary grid nodes. The position $\mathbf{x} = \mathbf{0}$ corresponds to a grid node adjacent to, but not at the boundary of the computational domain. The time $t = 0$ corresponds to the current time step. The derivative $f'(0)$ and the wave propagation vector $\mathbf{l}$ are estimated using Equations (40) and (41). Details on how this has been implemented are given in Section 3. A Cartesian grid is considered where the scalar variables are stored at the central nodes, but the velocity components are stored at staggered nodes. The method could also have been implemented on a colocated grid.

3. DERIVATION OF PLANE-WAVE BOUNDARY CONDITIONS ON A STAGGERED GRID

The Taylor expansions given by Equations (37)–(39) are implemented on a Cartesian grid. The derivative $f'(0)$ and the wave propagation vector $\mathbf{l}$ are estimated using Equations (40) and (41). The case of an open boundary with outward normal pointing in the positive x-direction is

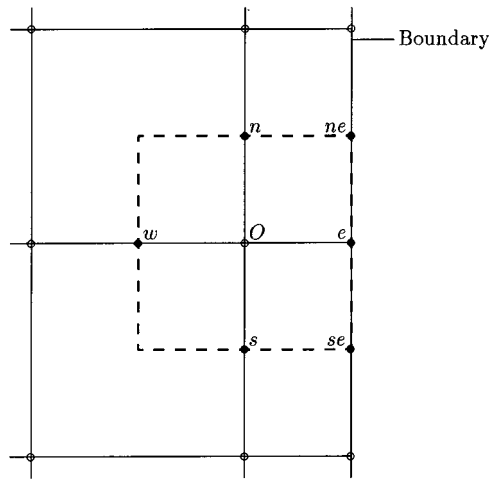

Figure 1. Geometry of the numerical grid at the boundary in the positive x-direction. Grid nodes in the xy-plane are shown. The scalar variables p, ρ, c, are stored at the central node O and the boundary node e. The velocity component u is stored at the staggered node w and the boundary node e. The velocity component v is stored at the staggered nodes n, s, and the staggered boundary nodes ne, se. The velocity component w is stored in a similar manner as v, but in the xz-plane. In this case the node n (north) in the positive y-direction is replaced by the node t (top) in the positive z-direction, and similarly, ne, s, se are replaced by te, b, be, respectively.

considered (see Figure 1). The scalar variables are stored at the central node, but the velocity components are stored at staggered nodes. Boundaries with normals in other directions are treated in a similar manner.

In the following analysis $\mathbf{x} = \mathbf{0}$ corresponds to the staggered node w where the velocity component u is stored. Values from three different time steps are considered. The superscripts n, $n-1$, $n+1$, correspond to values at the current time step, previous time step and next time step, respectively; $t = 0$ corresponds to the current time step.

The partial derivative $\partial/\partial t\, u(\mathbf{0}, 0)$ is approximated by

$$\frac{\partial}{\partial t} u(\mathbf{0}, 0) = \frac{u_w^n - u_w^{n-1}}{t^n - t^{n-1}}. \tag{42}$$

The following approximations are employed

$$\frac{\partial}{\partial t} v(\mathbf{0}, 0) = \frac{(v_s^n - v_s^{n-1}) + (v_n^n - v_n^{n-1})}{2(t^n - t^{n-1})}, \tag{43}$$

$$\frac{\partial}{\partial t} w(\mathbf{0}, 0) = \frac{(w_b^n - w_b^{n-1}) + (w_t^n - w_t^{n-1})}{2(t^n - t^{n-1})}. \tag{44}$$

These approximations may be justified by differentiating the expression for $\mathbf{u}(\mathbf{x}, t)$ in Equation (36), giving

$$\frac{\partial}{\partial t} \mathbf{u}(\mathbf{x}, t) = \frac{\mathbf{l}}{\rho_0 c_0} f'\left(t - \frac{\mathbf{l}\cdot\mathbf{x}}{c_0}\right). \tag{45}$$

Provided that the function f' is smooth enough

$$\frac{\partial}{\partial t} \mathbf{u}(\mathbf{x}, 0) = \frac{\mathbf{l}}{\rho_0 c_0} f'\left(-\frac{\mathbf{l}\cdot\mathbf{x}}{c_0}\right) = \frac{\mathbf{l}}{\rho_0 c_0}\left(f'(0) + O\left(\frac{|\mathbf{x}|}{c_0}\right)\right). \tag{46}$$

Thus, it is seen that

$$\frac{\partial}{\partial t} \mathbf{u}(\mathbf{x}, 0) = \frac{\partial}{\partial t} \mathbf{u}(\mathbf{0}, 0) + \frac{\mathbf{l}}{\rho_0 c_0} O\left(\frac{|\mathbf{x}|}{c_0}\right). \tag{47}$$

In accordance with Equation (40), the components of the normalized wave propagation direction $\mathbf{l}$ are determined by

$$l_i = \frac{\operatorname{sgn}(f'(0))\, \partial/\partial t\, u_i(\mathbf{0}, 0)}{|\partial/\partial t\, \mathbf{u}(\mathbf{0}, 0)|}, \quad i = 1, 2, 3. \tag{48}$$

The subscripts 1, 2, 3, correspond to components in the x-, y-, z-directions, respectively. The function $\operatorname{sgn}(\xi)$ is defined as 1 when $\xi \geq 0$, and -1 otherwise. In the numerical calculations we use

$$\operatorname{sgn}(f'(0)) = \operatorname{sgn}(\rho_O^n - \rho_O^{n-1}), \tag{49}$$

utilizing the fact that $f'(0) = c_0^2\, \partial/\partial t\, \rho(\mathbf{0}, 0)$ from Equation (35). Again, using Equation (40), the derivative $f'(0)$ is determined by

$$f'(0) = \operatorname{sgn}(f'(0)) \rho_O^n c_O^n \left|\frac{\partial}{\partial t} \mathbf{u}(\mathbf{0}, 0)\right|. \tag{50}$$

In the numerical calculations ρ_O^n and c_O^n are functions of time.

In the case of the velocity component u, the Taylor expansion of $\mathbf{u}(\mathbf{x}, t)$ in Equation (39) can now be applied directly to obtain

$$u_e^{n+1} = u_w^n + \frac{l_1 f'(0)((t^{n+1} - t^n) - (l_1 \Delta x)/c_O^n)}{\rho_O^n c_O^n}, \tag{51}$$

where Δx is the length of the control volume in the x-direction, i.e. the distance between the nodes w and e. Since the velocity components v and w are stored in other staggered nodes than u, Equation (39) cannot be applied directly in this case. First set $\mathbf{x} = \mathbf{x}_1$ in this equation and then $\mathbf{x} = \mathbf{x}_2$, $t = 0$, and subtract the second equation from the first to obtain

$$\mathbf{u}(\mathbf{x}_1, t) = \mathbf{u}(\mathbf{x}_2, 0) + \mathbf{l}\left(\frac{f'(0)}{\rho_0 c_0}\left(t - \frac{\mathbf{l}\cdot(\mathbf{x}_1 - \mathbf{x}_2)}{c_0}\right) + O\left(t^2, \frac{|\mathbf{x}_1|^2}{c_0^2}, \frac{|\mathbf{x}_2|^2}{c_0^2}\right)\right). \tag{52}$$

This modified Taylor expansion can now be applied to obtain

$$v_{se}^{n+1} = v_s^n + \frac{l_2 f'(0)((t^{n+1} - t^n) - (l_1 \Delta x)/2c_O^n)}{\rho_O^n c_O^n}, \tag{53}$$

$$w_{be}^{n+1} = w_b^n + \frac{l_3 f'(0)((t^{n+1} - t^n) - (l_1 \Delta x)/2c_O^n)}{\rho_O^n c_O^n}. \tag{54}$$

Note that the distance between the staggered node s (b) and the staggered boundary node se (be) is $0.5\Delta x$.

In the case of the pressure and the density, the Taylor expansions (37) and (38) are modified in a similar manner as shown in Equation (52)

$$p(\mathbf{x}_1, t) = p(\mathbf{x}_2, 0) + f'(0)\left(t - \frac{\mathbf{l}\cdot(\mathbf{x}_1 - \mathbf{x}_2)}{c_0}\right) + O\left(t^2, \frac{|\mathbf{x}_1|^2}{c_0^2}, \frac{|\mathbf{x}_2|^2}{c_0^2}\right), \tag{55}$$

$$\rho(\mathbf{x}_1, t) = \rho(\mathbf{x}_2, 0) + \frac{f'(0)}{c_0^2}\left(t - \frac{\mathbf{l}\cdot(\mathbf{x}_1 - \mathbf{x}_2)}{c_0}\right) + O\left(t^2, \frac{|\mathbf{x}_1|^2}{c_0^2}, \frac{|\mathbf{x}_2|^2}{c_0^2}\right). \tag{56}$$

Application of these two modified Taylor expansions leads to

$$p_e^{n+1} = p_O^n + f'(0)\left((t^{n+1} - t^n) - \frac{l_1 \Delta x}{2c_O^n}\right), \tag{57}$$

$$\rho_e^{n+1} = \rho_O^n + f'(0)\left(\frac{(t^{n+1} - t^n) - (l_1 \Delta x)/2c_O^n}{(c_O^n)^2}\right). \tag{58}$$

Note that when implementing the plane-wave boundary conditions, no knowledge of the ambient states assumed in the plane-wave relations in Equations (34)–(36) is needed. The fact that v_{se}^{n+1}, w_{be}^{n+1} are considered in this implementation and not v_{ne}^{n+1}, w_{te}^{n+1} is a choice that we have made. Instead, v_{ne}^{n+1}, w_{te}^{n+1} could have been considered, giving similar results. The important thing when the plane-wave boundary conditions are implemented in the numerical code, is that the value for the next time step of the v-velocity (w-velocity) at each boundary node is computed (a loop over all the control volumes adjacent to the considered boundary of the computational domain). Other ways of implementing the basic idea of the plane-wave boundary conditions are possible. Note that these boundary conditions are employed only when the wave propagation vector $\mathbf{l}$ is either parallel with the boundary or pointing out of the computational domain. When the wave propagation vector is pointing into the computational domain or when the norm of $\partial/\partial t\ \mathbf{u}(\mathbf{0}, 0)$ is very small (below a fixed small value), other boundary conditions are used. In this study, these are the characteristic boundary conditions

based on the theory of characteristics employed on the reduced, one-dimensional problem of flow perpendicular to the boundary [4,11]. These conditions employ zero-order extrapolation in space of the characteristic variables $(p - \rho_0 c_0 u)$, $(p - c_0^2 \rho)$, $(p + \rho_0 c_0 u)$ (obtained from Equation (6), assuming that the coefficient matrices are locally constant, subscript 0 denotes locally constant values) with one modification: for subsonic flow there is at least one incoming mode, implying that at least one condition must be set at the boundary. The approach chosen is such that this condition is given by $p = p_{\text{const}}$ at the boundary, i.e. the boundary pressure has a constant value, usually the ambient pressure (an exception is in the shock tube problem used as a test problem in the next section, here the boundary pressure is set to the value from the previous time step). When the code switches over to the characteristic conditions the boundary pressure gradually approaches the constant pressure defined in the characteristic conditions, to ensure a smooth transition. Note that the plane-wave boundary conditions are not employed when the flow is stationary. In this case $\partial/\partial t\ \mathbf{u}(\mathbf{0}, 0) = \mathbf{0}$ and no wave propagation direction can be determined.

4. RESULTS OF TEST CALCULATIONS

The plane-wave boundary conditions are tested for one-, two- and three-dimensional flow. A shock tube problem is considered where results using the plane-wave boundary conditions are compared with results using the non-linear, non-reflecting boundary conditions of Thompson. Furthermore, a single wave traveling in one and two dimensions is considered. In the one-dimensional case, a comparison is made with the results using the conditions of Thompson. Two blast waves intersecting each other at a right angle in two dimensions are also simulated. An example of a multiblock simulation of a blast wave from a gas explosion in three dimensions using the plane-wave boundary conditions is also shown. The plane-wave conditions behave similarly using the FLACS solver compared with the blast solver (cf. Section 1). In the numerical results shown here, the FLACS solver is employed in the one-dimensional simulations, and in the central block in the case where a gas explosion in a module is simulated. Otherwise the blast solver is employed. Practical use of the plane-wave boundary conditions in three-dimensional simulations is also reported in Reference [2].

4.1. Shock tube problem

In the shock tube problem, a long one-dimensional tube is divided into low- and high-pressure regions, separated by a diaphragm. At a time equal to zero, the diaphragm is instantly removed and a pressure discontinuity travels toward the low-pressure region and a rarefaction wave travels toward the high-pressure region. The detailed solution of the shock tube problem can be found in Reference [8]. In this study, at time of zero, the temperature is 293 K uniformly, and the velocity is zero uniformly. The pressure at the right side of the diaphragm is 100 kPa, at the left side 200 kPa. From the ideal gas relation for air, it is then found that the density at the right side is 1.19 kg m^{-3}, at the left 2.39 kg m^{-3}. The specific heat ratio γ is 1.4. The length of the computational domain is 1 m, and the diaphragm is in the middle of the tube before it is removed. The grid resolution is 200 control volumes of uniform length. Plots of velocity, pressure and density are shown as a function of position at $t = 1.0$ ms, and $t = 1.6$ ms. It is seen from the plots at $t = 1.0$ ms, see Figure 2, that the constant levels of the exact solution are quite well represented by the numerical solution, but the numerical solutions are smeared out at the discontinuities of the exact solution because a first-order upwind

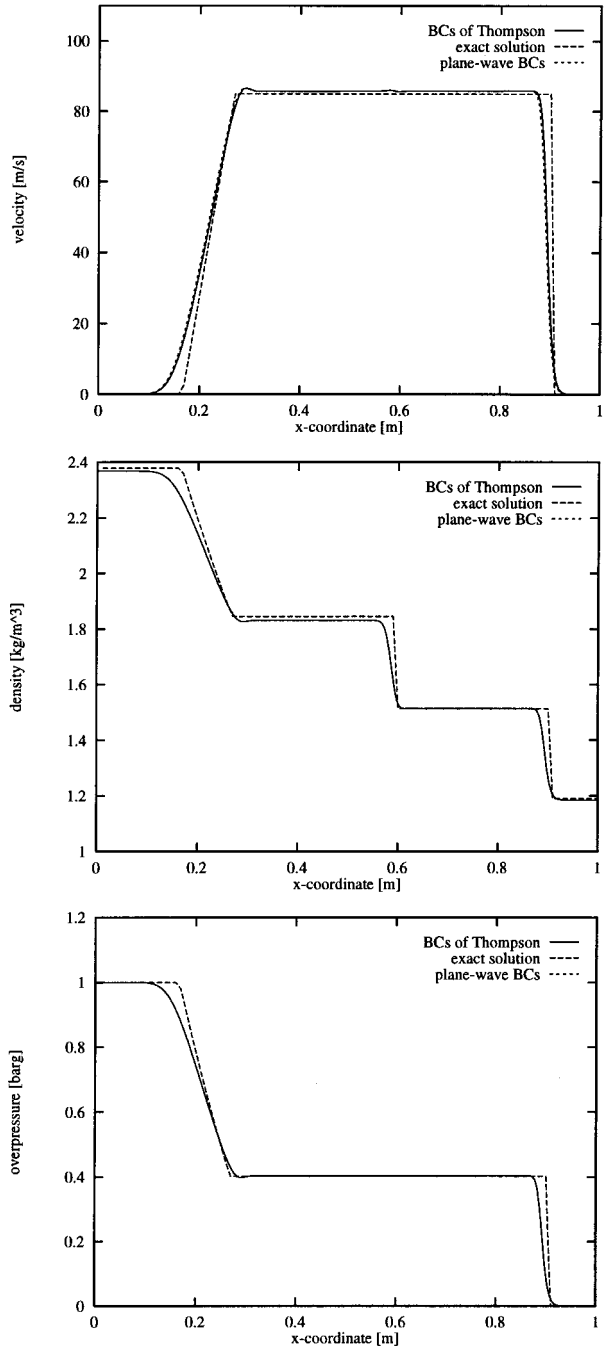

Figure 2. Shock tube for air, $\gamma = 1.4$, with initial conditions $u = 0$, $T = 293$ K uniformly, $p = 200$ kPa in high-pressure region ($x < 0.5$ m), $p = 100$ kPa in low-pressure region ($x > 0.5$ m). Overpressure (pressure minus 1.0 bar), density, velocity, as function of position at $t = 1.0$ ms. No wave (shock wave or rarefaction wave) has reached the boundary of the computational domain. The results are the same using the boundary conditions of Thompson compared with the plane-wave conditions.

scheme is used in our FLACS solver. The purpose of this exercise is, however, not to see how well the discontinuity can be represented, but to show how the numerical boundary conditions presented here are performing. Neither the shock wave nor the rarefaction wave has yet reached the boundary of the computational domain at $t = 1.0$ ms. No difference is seen between the results using the boundary conditions of Thompson, and the results using the plane-wave conditions. At $t = 1.6$ ms (see Figure 3), both the rarefaction wave and the shock wave have reached the boundary of the computational domain. Results using the non-linear, non-reflecting boundary conditions of Thompson are different compared with results with the plane-wave conditions. The numerical results near the boundary in the positive direction are somewhat better using the conditions of Thompson.

4.2. A single blast wave in one dimension

A one-dimensional blast wave in air, $\gamma = 1.4$, traveling in the positive x-direction, is considered. The computational domain is 70 m long. The grid resolution is one control volume per meter. The initial conditions at $t = 0$ for $x > 0$ are $u = 0$, $p = p_0 = 1$ bar, $T = 293$ K, uniformly. To simulate a blast wave entering the computational domain at $t = 0$, the pressure, density and velocity at the inlet $x = 0$ are set to

$$p_{\text{inlet}} = \begin{cases} p_s + (p_0 - p_s)\dfrac{t}{\Delta t_s} & \text{when } 0 \le t \le \Delta t_s \\ p_0 & \text{when } \Delta t_s < t, \end{cases} \tag{59}$$

$$\rho_{\text{inlet}} = \begin{cases} \rho_s + (\rho_0 - \rho_s)\dfrac{t}{\Delta t_s} & \text{when } 0 \le t \le \Delta t_s \\ \rho_0 & \text{when } \Delta t_s < t, \end{cases} \tag{60}$$

$$u_{\text{inlet}} = \begin{cases} u_s - u_s\dfrac{t}{\Delta t_s} & \text{when } 0 \le t \le \Delta t_s \\ 0 & \text{when } \Delta t_s < t. \end{cases} \tag{61}$$

Here, $\Delta t_s = 60$ ms is the duration of the blast wave and $\rho_0 = 1.19$ kg m^{-3} is the ambient density (computed from ideal gas law for air at ambient pressure, temperature). The boundary conditions at the open boundary in the positive x-direction are either the boundary conditions of Thompson or the plane-wave conditions.

It can be shown from the shock relations that the density ρ_s and the velocity u_s are given in terms of the pressure p_s, the ratio of specific heat γ, and the ambient entities, by

$$\rho_s - \rho_0 = \frac{p_s - p_0}{((\gamma - 1)p_s + (\gamma + 1)p_0)/2\rho_0}, \tag{62}$$

$$u_s = \frac{p_s p_0}{\rho_0\sqrt{\gamma(p_s + p_0)/(\rho_s + \rho_0)}}\frac{\rho_s + \rho_0}{\rho_s(\sqrt{\rho_0/\rho_s} + \sqrt{\rho_s/\rho_0})}. \tag{63}$$

In the limit of a weak shock, $p_s \to p_0$, it is seen that

$$\rho_s - \rho_0 \approx \frac{p_s - p_0}{\gamma(p_0/\rho_0)} = \frac{p_s - p_0}{c_0^2}, \tag{64}$$

$$u_s \approx \frac{p_s - p_0}{\rho_0\sqrt{\gamma(p_0/\rho_o)}} = \frac{p_s - p_0}{\rho_0 c_0}, \tag{65}$$

are relations of linear acoustics, cf. the relations stated for a plane traveling wave in Equations (34)–(36).

In one case, a compression wave with overpressure $(p_s - p_0) = 10$ kPa is considered. In Figure 4 the results are shown at different times for both the use of plane-wave boundary

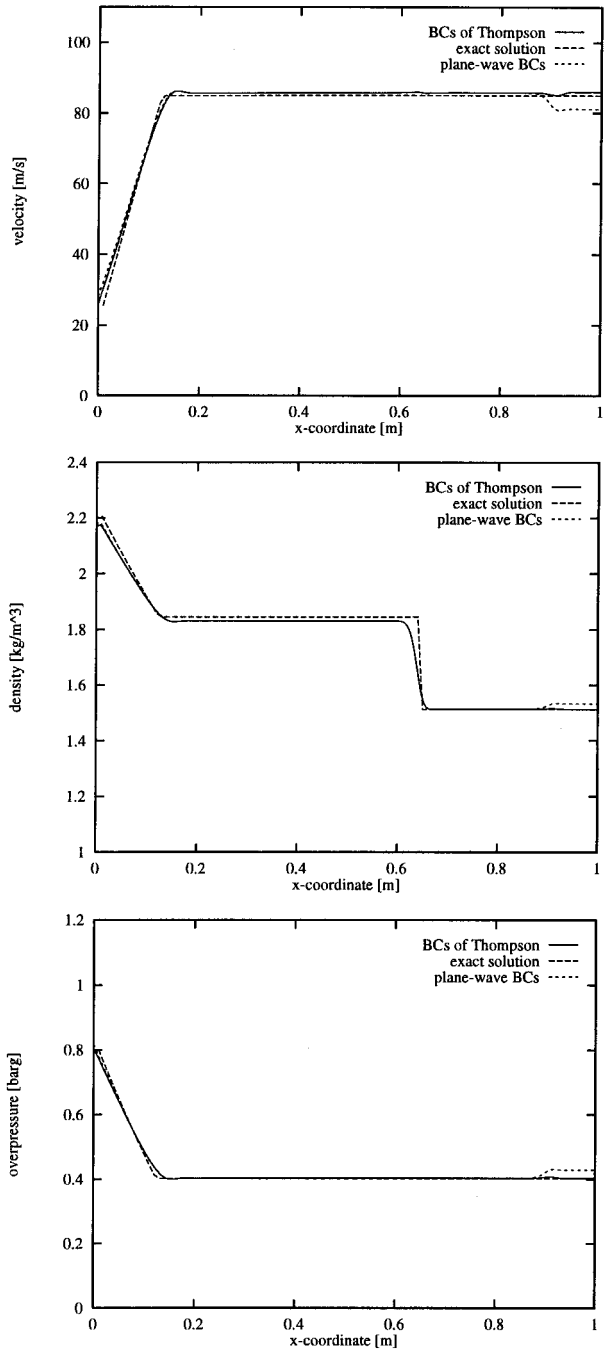

Figure 3. Shock tube for air, $\gamma = 1.4$, with initial conditions $u = 0$, $T = 293$ K uniformly, $p = 200$ kPa in high-pressure region ($x < 0.5$ m), $p = 100$ kPa in low-pressure region ($x > 0.5$ m). Overpressure (pressure minus 1.0 bar), density, velocity, as function of position at $t = 1.6$ ms. Both the rarefaction wave and the shock wave have reached the boundary of the computational domain. The results near the boundary in positive direction are somewhat better using the boundary conditions of Thompson compared with the plane-wave conditions.

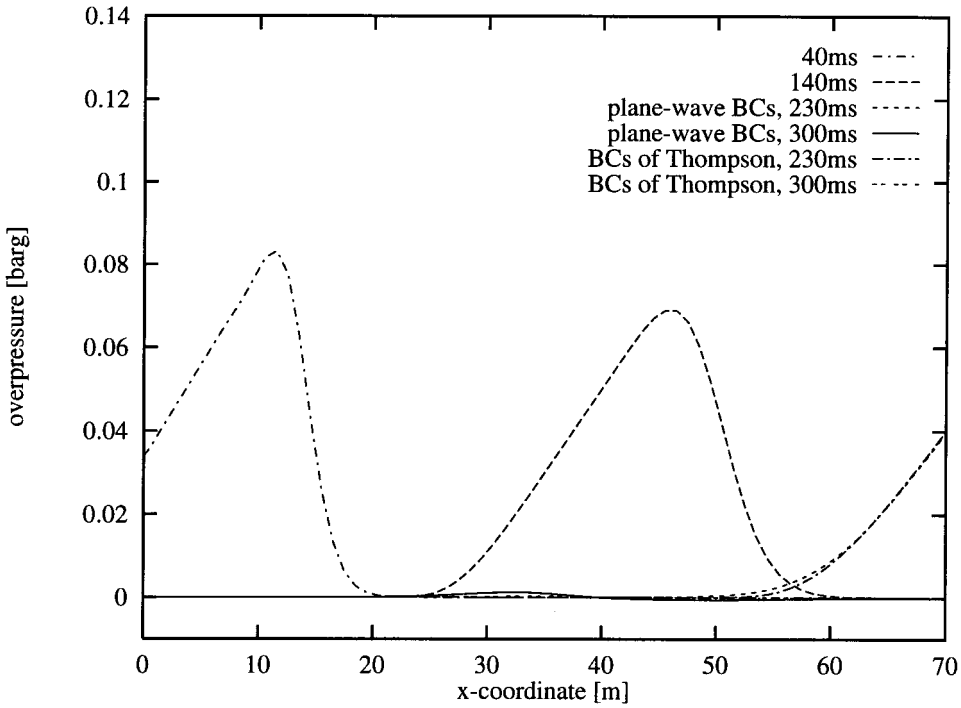

Figure 4. One-dimensional compression-wave propagation in air, $\gamma = 1.4$, with initial conditions $u = 0$, $T = 293$ K, $p = p_0 = 100$ kPa for $x > 0$. At $t = 0$, $x = 0$, a propagating wave enters the computational domain, the overpressure is $(p_s - p_0) = 10$ kPa, with a linear decay down to zero within 60 ms, cf. Equations (59)–(61). Negligible artificial reflection at open boundary in positive direction using the plane-wave boundary conditions, or the boundary conditions of Thompson.

conditions and the non-linear conditions of Thompson. In both cases the artificially reflected wave is negligible. Similar results are seen in another numerical simulation with overpressure $(p_s - p_0) = 100$ kPa (see Figure 5).

4.3. A single blast wave in two dimensions

A two-dimensional simulation of a single blast wave with overpressure $(p_s - p_0) = 10$ kPa has also been performed using the plane-wave boundary conditions. The computational domain is 70×30 m, one control volume covering 1×1 m. This case is similar to the one-dimensional cases considered in Section 4.2, except that the wave propagates at a 45° angle relative to the co-ordinate axes (see Figure 6).

No reflection from the open boundary can be seen from these plots. The contour lines are not exactly straight lines, but slightly curved. This is due to numerical smearing of the front and non-linear effects (the boundary conditions on the two sides where the plane wave enters the computational domain are set as if it is exactly a linear plane wave entering, and inlet values are set according to Equations (59)–(61)). At $t = 300$ ms the blast wave has left the computational domain. The absolute value of the overpressure is now less than 2.5% of the maximum overpressure of the incoming wave (contour plot at $t = 300$ ms not shown here).

4.4. Two blast waves intersecting each other at a right angle

With the plane-wave boundary conditions the flow field is locally approximated by a single plane wave. In general a flow field cannot be represented that simply. An example of this is two plane waves crossing each other at a right angle. This case is considered analytically in Reference [11], where a so-called formal expansion based on the assumption of a single plane traveling wave is compared with a Taylor expansion. Numerical results are shown of two blast waves crossing each other at a right angle using the plane-wave boundary conditions. One blast wave is propagating in the positive x-direction, the other in the positive y-direction. Both waves enter at $t = 0$, the computational domain being 70 m in the x-direction and 30 m in the y-direction. Each control volume of the numerical grid covers 1×1 m. The overpressure $(p_s - p_0)$ is 10 kPa for both waves with a linear decay down to zero overpressure within 60 ms, cf. Equations (59)–(61). The results are for air, $\gamma = 1.4$, with initial conditions $(u, v) = (0, 0)$, $T = 293$ K, $p = p_0 = 100$ kPa.

In Figure 7(a) a contour plot of the overpressure is shown at $t = 70$ ms. It is seen that the two waves interact, and the wave propagating in the y-direction is just about to start leaving the computational domain. In Figure 7(b) the situation at $t = 145$ ms is shown when the wave traveling in the y-direction has just left the computational domain. It is seen that the wave traveling in the x-direction is partly distorted. This is due to a non-linear interaction between the two blast waves when they cross each other, and effects related to the boundary conditions.

At $t = 300$ ms both blast waves have left the computational domain. The absolute value of the overpressure is now 4% or less of the maximum overpressure of the incoming waves

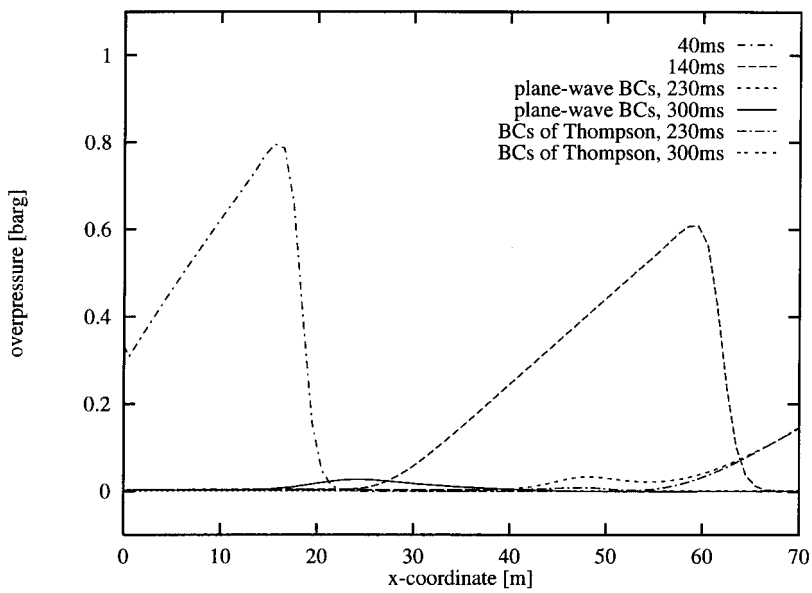

Figure 5. One-dimensional compression-wave propagation in air, $\gamma = 1.4$, with initial conditions $u = 0$, $T = 293$ K, $p = p_0 = 100$ kPa for $x > 0$. At $t = 0$, $x = 0$, a propagating wave enters the computational domain, the overpressure is $(p_s - p_0) = 100$ kPa, with a linear decay down to zero within 60 ms, cf. Equations (59)–(61). Negligible artificial reflection at open boundary in positive direction using the plane-wave boundary conditions, or the boundary conditions of Thompson.

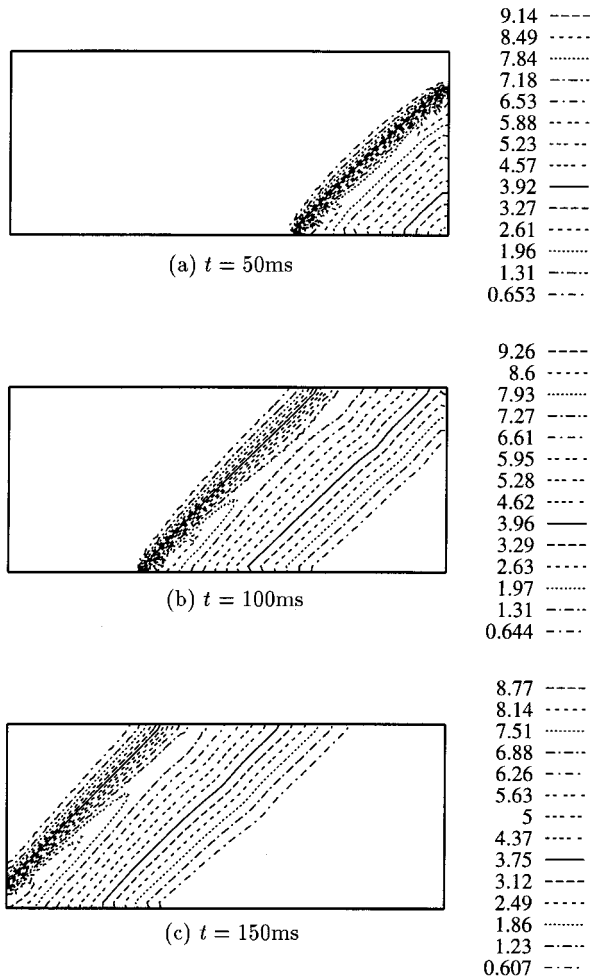

Figure 6. Two-dimensional blast-wave propagating at a 45° angle relative to the co-ordinate axes, the computational domain is 70×30 m. The results are for air, $\gamma = 1.4$, with initial conditions $(u, v) = (0, 0)$ $T = 293$ K, $p = p_0 = 100$ kPa. At $t = 0$ a propagating wave enters the computational domain, the overpressure is $(p_s - p_0) = 10$ kPa, with a linear decay down to zero within 60 ms, cf. Equations (59)–(61). Contour-plots of the overpressure (kPa) at different moments, (a) at $t = 50$ ms, (b) at $t = 100$ ms, (c) at $t = 150$ ms. No reflection from the open boundary is seen using the plane-wave boundary conditions.

(contour plot at $t = 300$ ms not shown here). Thus, even in the difficult case of two blast waves crossing each other at a right angle, the relative error due to effects of the boundary conditions, is limited.

4.5. Blast wave from gas explosion in three dimensions

An example is given of practical use of the plane-wave boundary conditions in three dimensions. Here an explosion in a compressor module is simulated. A combustible cloud

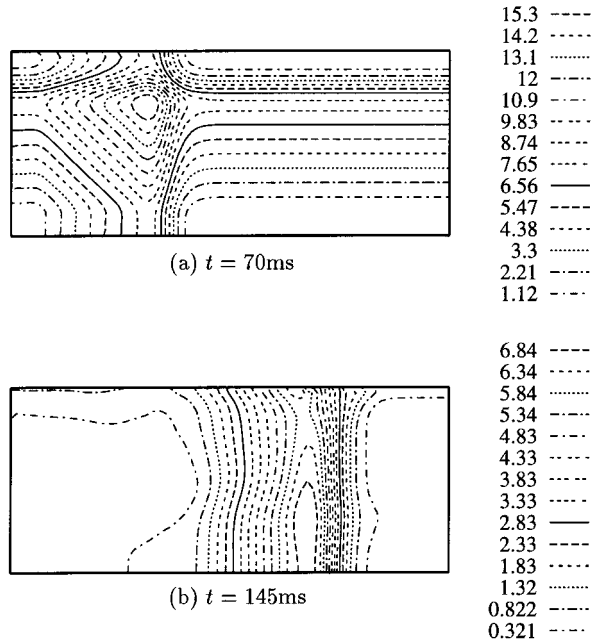

Figure 7. Two-dimensional simulation of two blast waves crossing each other at a right angle using the plane-wave boundary conditions. The computational domain is 70×30 m. The results are for air, $\gamma = 1.4$, with initial conditions $(u, v) = (0, 0)$, $T = 293$ K, $p = p_0 = 100$ kPa. At $t = 0$ a propagating wave enters the computational domain in the positive x-direction and another wave in the positive y-direction, for both waves the overpressure is $(p_s - p_0) = 10$ kPa, with a linear decay down to zero within 60 ms, cf. Equations (59)–(61). Contour-plots of the overpressure (kPa) at different moments, (a) at $t = 70$ ms when the two waves interact, (b) at $t = 145$ ms when the wave propagating upward has left the computational domain.

filling the whole module is ignited in the central part. In Figure 8 pressure contours are shown in a horizontal cut plane. The outgoing blast wave from the central part of the explosion is shown. Several blocks are used in the simulation. Note that no artificial reflections are seen from the boundary of the computational domain.

5. CONCLUSIONS

Boundary conditions based on a local approximation by a plane traveling wave have been presented. The derivation of these boundary conditions was presented in detail. The plane-wave boundary conditions are conceptually simple and are easy to implement in several dimensions. In the numerical experiments involving propagating waves it has been shown that the method yields negligible artificial reflections from open boundaries. The method has been implemented in a three-dimensional CFD code for simulations of gas explosions and blast-wave propagation in complex geometries.

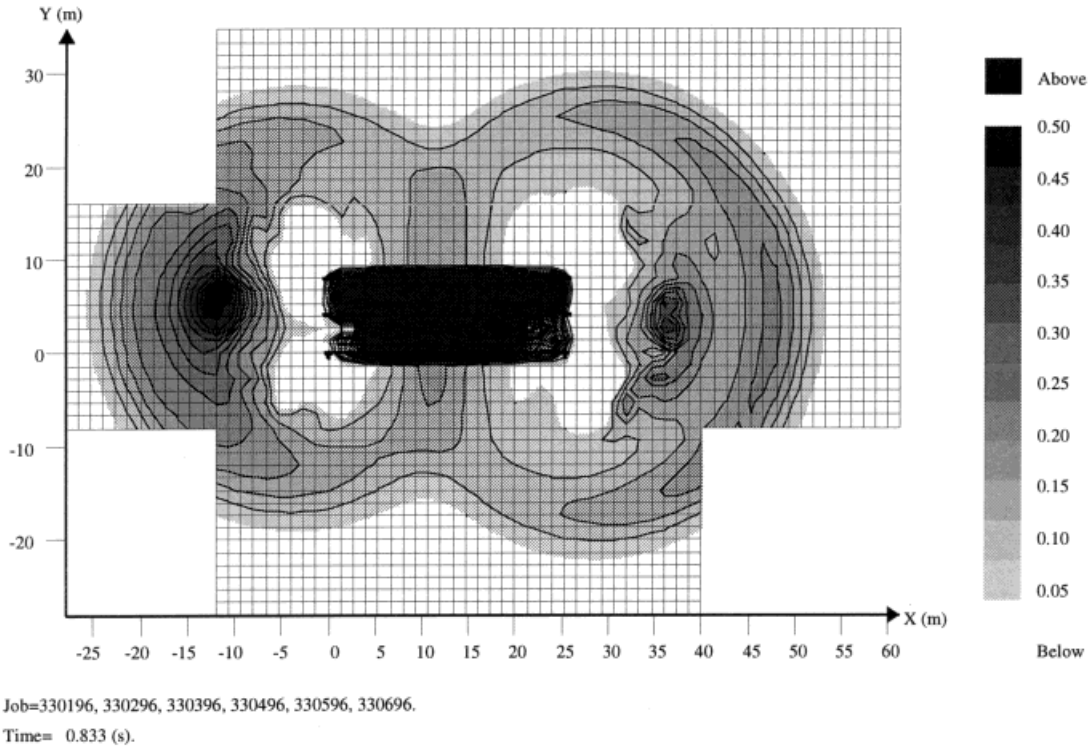

Figure 8. Example of three-dimensional multiblock simulation of gas explosion and blast-wave propagation with the CFD code FLACS. A combustible cloud filling the whole compressor module is ignited in the central part. Contour plot of overpressure (bar) in horizontal plane close to the ground. No artificial reflections are seen from the boundary of the computational domain using the plane-wave boundary conditions.

ACKNOWLEDGMENTS

This work was supported by the Research Council of Norway through program number STP-30074, and by the following companies and authorities participating in the Gas Safety Programme 93-96: BP, HSE, Gaz de France, Elf, Esso, Mobil, NPD, Phillips and Statoil.

APPENDIX A. NOMENCLATURE

Latin letters	
c	speed of sound
$\mathbf{l}$	(l_1, l_2, l_3), wave propagation direction (unit vector)
p	pressure
s	entropy
t	time
T	temperature
$\mathbf{u}$	$(u, v, w) = (u_1, u_2, u_3)$, velocity
$\mathbf{x}$	(x, y, z), spatial co-ordinates
Greek letters	
Δx	length of control volume in the x-direction

γ	ratio of specific heats, c_p/c_v
ρ	density

Subscripts

0	ambient value, or locally constant value
s	shock value (Section 4)

Superscripts

$n-1$	previous time step
n	current time step
$n+1$	next time step

REFERENCES

1. K. Van Wingerden, I.E. Storvik, B.J. Arntzen, R. Teigland, J.R. Bakke, I.Ø. Sand and H.R. Sørheim, 'FLACS-93, a new explosion simulator', *2nd Int. Conf. on Offshore Structural Design Against Extreme Loads*, London, 1993.
2. K. Van Wingerden, O.R. Hansen and R. Teigland, 'Prediction of the strength of blast waves in the surroundings of vented offshore modules', *Proc. 4th Int. Conf. and Exhibition on Offshore Structures—Hazards, Safety and Engineering*, ERA Report 95-1173, London, 1995, pp. 2.1.1–2.1.13.
3. S.V. Patankar and D.B. Spalding, 'A calculation procedure for heat, mass and momentum transfer in three-dimensional parabolic flows', *Int. j. heat mass transfer*, **15**, 1787–1806 (1972).
4. J.R. Bakke, 'Numerical simulation of gas explosions in two-dimensional geometries', *CMI Report No. 865403-8*, Chr. Michelsen Institute, Bergen, Norway, 1986.
5. F.H. Harlow and A.A. Amsden, 'A numerical fluid dynamics calculation method for all flow speeds', *J. Comput. Phys.*, **8**, 197–213 (1971).
6. D.L. Book, *Finite-Difference Techniques for Vectorized Fluid Dynamics Calculations*, Springer, New York, 1981.
7. R. Hixon, S.-H. Shih and R.R. Mankbadi, 'Evaluation of boundary conditions for computational aeroacoustics', *AIAA J.*, **33**, 2006–2012 (1995).
8. C. Hirsch, *Numerical Computation of Internal and External Flows*, Vol. 2, Wiley, Chichester, 1990.
9. K.W. Thompson, 'Time dependent boundary conditions for hyperbolic systems', *J. Comput. Phys.*, **68**, 1–24 (1987).
10. A.D. Pierce, *Acoustics: An Introduction to its Physical Principles and Applications*, McGraw-Hill, New York, 1981.
11. H.-C. Salvesen and R. Teigland, 'Nonreflecting boundary conditions based on local approximation by a plane wave', *CMR-96-A20062(I)*, Christian Michelsen Research, Bergen, Norway, 1996.

